CONDITIONAL MOMENT CLOSURE MODELLING OF SOOT FORMATION IN TURBULENT NON-PREMIXED, ETHYLENE-AIR FLAMES

Yunardi, Robert M. Woolley and Michael Fairweather
Energy and Resources Research Institute,
School of Process, Environmental and Materials Engineering,
University of Leeds, Leeds,
West Yorkshire, LS2 9JT, UK
r.m.woolley@leeds.ac.uk

ABSTRACT

Presented are results obtained from the incorporation of a semi-empirical soot model into a first-order Conditional Moment Closure (CMC) approach to modelling turbulent, non-premixed, ethylene-air flames. Soot formation is determined via the solution of two transport equations for the soot mass fraction and the particle number density, with acetylene and benzene employed as the incipient species responsible for soot nucleation. The concentrations of these species are calculated using a detailed gas-phase kinetic scheme involving 463 reactions and 70 species. The study focuses on the influence of differential diffusion of soot particles on soot volume fraction predictions, and the results of calculations are additionally compared with experimental data for the flow field and temperatures of the three ethylene-air flames investigated. Good agreement with soot data is found provided differential diffusion effects are included.

INTRODUCTION

Despite dwindling resources, fossil fuel combustion still plays a major role in the world economy and is widely used for the production of energy. The formation and emission of particulate pollutants such as soot, as a consequence of hydrocarbon combustion, is fast becoming a major concern in both developed and more so, developing countries. Within most combustion systems, soot formation and oxidation usually occurs in highly turbulent zones which involve the interaction of complex chemical and physical phenomena. In order to accurately predict the production and destruction of soot in such systems, an integrated model representing turbulence, the interaction between turbulence and gas-phase chemistry, soot particle production and removal, and radiation heat losses is required. The ability to apply such an integrated model of demonstrable accuracy to minimise soot production and emission in relation to safety and environmental considerations, would represent a major step-forward in our ability to design and manage combustion processes.

Soot particles are of significantly greater mass than gas-phase species, and therefore they diffuse considerably more slowly than the latter. However, the majority of models used in predicting soot in non-premixed turbulent flames assume equal diffusivity of soot particles and gas-phase species (Wen et al., 2003; Ma et al., 2005; Mauss et al., 2006). Kronenburg et al. (2000) were amongst the first to point out the importance of accounting for the differential diffusion of soot particles when predicting methane sooting flames. Pitsch et al. (2000) also obtained improved predictions of soot volume fractions in the context of ethylene non-premixed flames when the effects of differential diffusion were taken into consideration.

When predicting turbulent combustion, difficulty is encountered in modelling the chemical source term that appears in the species continuity equations. The highly non-linear dependence of this term on species concentrations and temperature, which fluctuate rapidly in turbulent flows, impedes any attempt at a linear first-order closure in terms of the averaged local temperature and concentrations. The CMC method addresses this problem by utilising moments conditioned on a value of a conserved scalar, namely the mixture fraction. Undertaking calculations in conserved scalar space allows the removal of much of the non-linearity of the chemical source term by assuming fluctuations due to turbulence to be negligible (Klimenko and Bilger, 1999).

First-order CMC has been applied in the form of a parabolic equation set to a wide range of combustion problems and has performed successfully for attached non-premixed jet flames (Fairweather and Woolley, 2003; 2004) and lifted turbulent jet diffusion flames (Kim and Mastorakos, 2005). In addition to these successes in modelling gas-phase combustion, CMC has also shown promise in the calculation of soot formation in non-premixed flames (Kronenburg et al., 2000).

In this paper, the results of an application of a first-order CMC approach (Klimenko and Bilger, 1999) to the calculation of turbulent non-premixed, ethylene-air flames and soot formation are presented. The soot model used in the calculations is based on that presented by Leung et al. (1991) and Lindstedt (1994), with transport equations for soot mass fraction and particle number density incorporated into the CMC approach. The influence of differential diffusion of soot particles, previously investigated by Kronenburg et al. (2000), is further assessed within the computation of these turbulent ethylene flames.

MATHEMATICAL MODELLING

Experimental Conditions and Flow Calculations

The three non-premixed ethylene-air flames considered in the present study have been experimentally reported by

Kent and Honnery (1987), Coppalle and Joyeux (1994), and Young and Moss (1995), denoted from now on as flames KH, CJ and YM. The important characteristics of each of these flames are presented in Table 1 and further details of the flame geometry, methods of data collection, and processing can be found in the relevant references.

Table 1: Operating conditions for ethylene-air flames

Ethylene-air flames	KH	CJ	YM
Absolute pressure/atm	1	1	1
Fuel exit velocity/m s^{-1}	52	29.5	24.5
Fuel exit temperature/K	322	322	293
Nozzle diameter/mm	3	4	3.1
Exit Reynolds number	14660	11100	8600
Co-flow air velocity/m s^{-1}	0	0	0

The calculation of the flow and mixing fields was achieved by solving the Favre-averaged forms of the partial differential equations which describe conservation of mass, momentum and the transport of mixture fraction and its variance. A standard *k-ε* turbulence model was used to close the above equation set. Standard turbulence modelling constants appropriate to axisymmetric flows were employed, although to ensure the accurate prediction of the spreading rate of the jets, an adjustment was made to the value of $C_{\varepsilon 2}$ from 1.92 to 1.84 to affect an increase in the dissipation rate of turbulence kinetic energy. A modified version of the GENMIX (Spalding, 1977) code was implemented in the solution of the two-dimensional, axisymmetric forms of the transport equations. The code applies an implicit formula in the stream-wise direction and a hybrid-differencing scheme in the cross-stream direction for its marching integration procedure.

First-Order CMC-Based Soot Model

A general first-order, parabolic CMC equation can be obtained by averaging the instantaneous equation governing species mass fraction, Y_i in statistically stationary, turbulent reacting flow, on the condition that the instantaneous mixture fraction ξ equals an arbitrary value η. Assuming a negligible variation in conditional statistics across the width of the flow, also allows the implementation of a one-dimensional form. However, in order to account for any small variations that may be present, the CMC equation can be radially averaged by integrating across the flow (Barlow et al., 1999). When the conserved scalar and reactive scalar have differing diffusion coefficients, that is $D_i \neq D_\xi$, an unclosed form of the CMC equation can be written for a conditional transported scalar (Q_i) as:

$$\frac{\partial Q_i}{\partial x}\langle u|\eta\rangle^* = \frac{1}{2}\frac{D_i}{D_\xi}\langle\chi|\eta\rangle^*\frac{\partial^2 Q_i}{\partial\eta^2} + \left(\frac{D_i}{D_\xi}-1\right)\left\langle\frac{\partial}{\partial x}\left(\rho D_\xi\frac{\partial\xi}{\partial x}\right)\middle|\eta\right\rangle^*\frac{\partial Q_i}{\partial\eta} + \langle\omega_i|\eta\rangle + e_{y,i} \quad (1)$$

For the derivation of the conditional gas-phase species mass fraction equation, both reactive and conserved scalars are assumed to diffuse equally, which implies $D_i = D_\xi$. With this assumption, the second and last terms on the right hand-side of Eq. 1, representing the source terms that generate differential and spatial diffusion, respectively, are cancelled. The conditional scalar dissipation ($\langle\chi|\eta\rangle$) was modelled using the approach of Girimaji (1991), while the remaining non-linear chemical source term $\langle\omega_i|\eta\rangle$ was modelled as for simple first-order closure, assuming the conditional fluctuations of the reactive scalars around the mean to be negligible. Mean values were obtained using the CHEMKIN package (Kee et al., 1996), together with a full chemical kinetic scheme consisting of 70 species and 463 reactions (Qin et al., 2000).

In addition to the CMC species transport equation, the soot model employed in the present study, as described in Leung et al. (1991) and Lindstedt (1994), requires the solution of two additional transport equations for the soot mass fraction, Y_s, and the soot particle number density, N_s. In the case of differential diffusion being neglected, the transport equations for Y_s^+ and N_s^+ are obtained in a similar way as for the gas-phase species, setting $D_{Y_s^+} = D_{N_s^+} = D_\xi$ for $i = Y_s^+, N_s^+$ in Eq. 1, to give:

$$\frac{\partial Q_{Y_s}^+}{\partial x}\langle u|\eta\rangle^* = \frac{1}{2}\langle\chi|\eta\rangle^*\frac{\partial^2 Q_{Y_s}^+}{\partial\eta^2} + \langle\omega_{Y_s}|\eta\rangle \quad (2)$$

$$\frac{\partial Q_{N_s}^+}{\partial x}\langle u|\eta\rangle^* = \frac{1}{2}\langle\chi|\eta\rangle^*\frac{\partial^2 Q_{N_s}^+}{\partial\eta^2} + \langle\omega_{N_s}|\eta\rangle \quad (3)$$

where the superscript + refers to a scalar of equal diffusivity. When the differential diffusion of soot particles is taken into account, fixing the molecular coefficients of soot particles and nuclei equal to zero, i.e. $D_{Y_s} = D_{N_s} = 0$ for $i = Y_s, N_s$, Eq. 1 simplifies by neglecting the dissipation term, this being the first term on the right-hand side. However, the $e_{y,i}$ spatial diffusion terms seen in Eq. 1 now become significant. The current modelling approach follows the works of Kronenburg and Bilger (2001a, 2001b) in the representation of $e_{y,i}$, and the transport equations considering the effects of differential diffusion are modelled as Eqs. 4 and 5, where τ_K is the Kolmogorov time scale.

$$\frac{\partial Q_{Y_s}}{\partial x}\langle u|\eta\rangle^* = \left\langle\frac{\partial}{\partial x}\left(\rho D_\xi\frac{\partial\xi}{\partial x}\right)\middle|\eta\right\rangle^*\frac{\partial Q_{Y_s}}{\partial\eta} + \langle\omega_{Y_s}|\eta\rangle - 0.4\frac{\left(Q_{Y_s}-Q_{Y_s}^+\right)}{\tau_K(\eta)} \quad (4)$$

$$\frac{\partial Q_{N_s}}{\partial x}\langle u|\eta\rangle^* = \left\langle\frac{\partial}{\partial x}\left(\rho D_\xi\frac{\partial\xi}{\partial x}\right)\middle|\eta\right\rangle^*\frac{\partial Q_{N_s}}{\partial\eta} + \langle\omega_{N_s}|\eta\rangle - 0.4\frac{\left(Q_{N_s}-Q_{N_s}^+\right)}{\tau_K(\eta)} \quad (5)$$

The source terms $\langle \omega_{Y_s} | \eta \rangle$ in Eqs. 2 and 4 account for the effects of soot nucleation, surface growth and oxidation. Acetylene and benzene were selected as the incipient species responsible for soot nucleation (Lindstedt, 1994). However, the former species was considered as the only chemical contributor to the increase in soot mass via surface growth. The soot nucleation proceeds via the reactions $C_2H_2 \leftrightarrow 2C_s + H_2$ and $C_6H_6 \leftrightarrow 6\,C_s + 3H_2$ and it is assumed that surface growth continues via an acetylene reaction similar to that of soot nucleation. Assuming soot oxidation to proceed through $C_s + 0.5\,O_2 \rightarrow CO$ and $C_s + OH \rightarrow CO + H$, the source term for the soot mass fraction equation can now be written as:

$$\begin{aligned}\langle \omega_{Y_s} | \eta \rangle = {} & 2k_1(Q_T)Q_{C_2H_2}M_s + 6k_2(Q_T)Q_{C_6H_6}M_s \\ & + k_3(Q_T)A_sQ_{C_2H_2}M_s - k_4(Q_T)A_sQ_{O_2}M_s \\ & - k_5(Q_T)A_sQ_{OH}M_s\end{aligned} \quad (6)$$

where M_s is the soot molecular weight.

The source terms $\langle \omega_{N_s} | \eta \rangle$ in Eqs. 3 and 5 represent the production and reduction of soot particle number density due to nucleation and agglomeration, respectively. With N_A representing the Avogadro number, C_a an agglomeration constant, σ_B the Stefan-Boltzmann constant, and $C_{\min}$ the minimum carbon atom number, they can be expressed as:

$$\begin{aligned}\langle \omega_{N_s} | \eta \rangle = {} & \left[2k_1(Q_T)Q_{C_2H_2} + 6k_2(Q_T)Q_{C_6H_6} \right] \frac{N_A}{C_{\min}} \\ & - 2C_a \left(\frac{6}{\pi} \frac{Q_{Y_s}}{\rho_\eta Q_{N_s}} \right)^{1/6} \left(\frac{6\sigma_B Q_T}{\rho_s} \right)^{1/2} \left(\rho_\eta Q_{N_s} \right)^2\end{aligned} \quad (7)$$

Reaction rate constants for nucleation, surface growth and oxidation that appear in Eqs. 6 and 7 are presented in Table 2 (Lindstedt, 1994; Kronenburg et al., 2000).

Solution of the CMC Equations

Flow and mixing field information from the turbulent flow calculations employing a reacting-flow density were passed to the CMC model, where the set of species mass fractions, soot mass fraction, particle number density and enthalpy equations were solved in mixture fraction space. The flow and mixing field are related to the reactive scalar field through the mean density, and comparison between densities obtained from the CMC solution and prescribed equilibrium values showed little variation at the locations examined in the flames considered. Coupling of the flow field and CMC calculations was therefore deemed unnecessary for the calculations reported. Solution of the CMC equations in real space was achieved using a fractional step method, implemented using the stiff ODE solver VODE (Brown et al., 1989), which applies a backward differentiation formula approach to the solution of the non-linear equation set. Second-order differential sample space terms were determined using a central differencing approximation. The computational grids consisted of 68 radial nodes in mixture fraction space.

Table 2: Reaction rate constants for soot formation and oxidation, in the form of the Arrhenius expression $k_j = AT^b \exp(-T_a/T)$ (units K, kmol, m, s).

k_j	A	b	T_a
k_1	1.0 x 10^4	0.0	21,000
k_2	0.75 x 10^5	0.0	21,000
k_3	0.75 x 10^3	0.0	12,100
k_4	7.15 x 10^2	0.5	19,680
k_5	3.60 x 10^{-1}	0.5	0

RESULTS AND DISCUSSION

Predicted and measured values of temperature along the centreline, and radially at three different heights above the burner, in flame KH are shown in Fig. 1. The temperature predictions display quantitatively good results in comparison to experimental data. It should be noted that the flat calculated axial temperature profile close to the nozzle indicates a region prior to CMC calculations commencing. It is seen that the progress of the computed axial temperature is in line with the measurements up to around 500 mm above the burner. Beyond this height, however, the temperature is over-predicted by up to 200 K in the furthermost downstream positions. This is consistent with the calculations of Ma et al. (2005) which used a flamelet approach with a k-ε turbulence closure, and Lindstedt and Louloudi (2005) who used a transported PDF approach.

Predicted radial temperatures at x = 138 and 241.5 mm downstream of the nozzle are in excellent agreement with data throughout the flame. Further downstream, at x = 345 mm, although the core and radial peak temperatures are well captured, the prediction in the fuel-lean region deviates somewhat from experimental results. At the same axial position, Pitsch et al. (2000) found that the calculated temperature over-predicted the radial data due to an overestimation of the jet spreading rate.

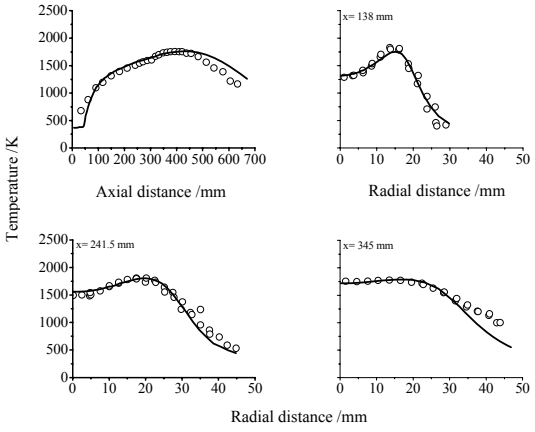

Fig. 1: Axial and radial temperature profiles for flame KH (symbol – measured, line – predicted).

The accuracy of the turbulent flow field prediction, in addition to the inclusion of the effects of radiation heat transfer into a combustion model, is of prime importance in order to correctly predict the temperature of a combustion system. A simple radiation model employed herein, where emissions from species CO_2, H_2O, CH_4, CO and soot were included, has been found to yield reasonable accuracy in many non-sooting combustion applications (Fairweather and Woolley, 2003; 2004). The precise prediction of peak temperatures obtained in both the centreline and radial directions, as shown in Fig. 1, indicates the method of accounting for soot radiation is satisfactorily implemented in this flame.

Predictions of axial and radial distributions of soot volume fraction are presented alongside experimental values in Fig. 2. The solid line represents the simulations resulting from considering the effect of differential diffusion, and the dashed line the simulations which neglected differential diffusion in the CMC calculation. When the assumption of equal diffusivity is applied, it is clearly seen that the centerline soot volume fraction profile is significantly under-predicted in the soot formation zone. The predicted soot formation starts at a lower rate than that measured, leading to a shift of peak soot volume fraction into the oxidation zone. The measured peak soot volume fraction of 1.57 x 10^{-6} is under-predicted by two orders of magnitude. A key issue is that the discrepancy between the computed and measured soot volume fraction in the formation zone is directly related to the modelling of the surface growth rate in the soot model. When the effect of differential diffusion is neglected, the approximation that the surface growth rate is proportional to the local soot surface area, $f(A_s) = A_s$, results in significantly low soot volume fractions, as observed by Lindstedt (1994) and Ma et al. (2005) in ethylene flames, and Kronenburg et al. (2000) in methane flames. However, when the differential diffusion between soot particles and gas-phase species is taken into account, the soot volume fraction prediction is brought in line with measurements. The magnitude of the peak soot volume fraction is slightly below the measured value, but the shape of the measured profile is very well captured in both the formation and oxidation zones.

Inspection of the radial profiles in Fig. 2 at the downstream locations of x = 241.5 and 345 mm indicates that poor agreement between prediction and measurement is obtained with the assumption of equal diffusivity. However, at axial positions x = 138 and x = 483 mm better agreement is obtained. Results based on the differential diffusion model are very encouraging. Overall, the shape of the radial soot volume fraction profile is precisely predicted. At the location closest to the nozzle, x = 138 mm, the predicted soot volume fraction reaches an off-axis peak, this finding being consistent with that of Ma et al. (2005) and Pitsch et al. (2000) who used a flamelet approach. The experimental data do not clearly display such a peak value, although Kent and Honnery (1987) do state that close to the nozzle the measured soot volume fractions exhibit off-axis peaks which approach the axis at x = 345 mm.

Turning to the second flame investigated, Fig. 3 presents axial profiles of temperature and soot volume fraction, as well as radial profiles of soot volume fraction at

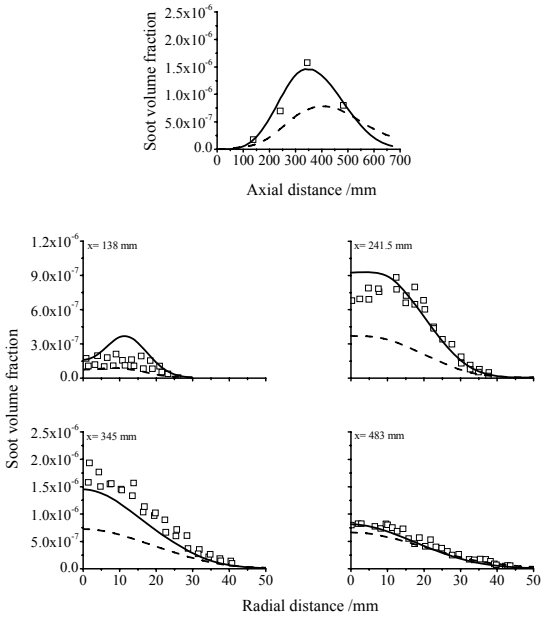

Fig. 2: Axial and radial soot volume fraction profiles for flame KH (symbol – measured, solid line – predicted with differential diffusion, dashed line – predicted neglecting differential diffusion).

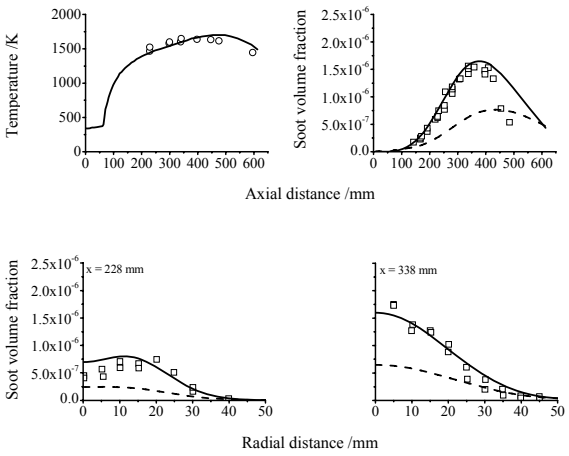

Fig. 3: Axial temperatures and soot volume fraction, and radial soot volume fraction profiles for flame CJ. Notation as in Fig. 2.

two different downstream locations, in flame CJ. Again, the results show that the predicted temperature is in excellent agreement with data, with temperatures captured along the centreline of the flame, and with good agreement in terms of the magnitude and location of the peak temperature. These results are in line with those achieved using the transported PDF method (Lindstedt and Louloudi, 2005), although it should be noted that no adjustment was made to the enthalpy source term in the present work in order to obtain

this level of agreement. Unfortunately, the experimental data lacks radial temperature profiles so comparisons in this regard are not possible.

Figure 3 also shows the centreline profile of soot volume fraction, indicating similar trends to those found in flame KH where neglecting the effect of differential diffusion yields lower predictions at all axial locations. Accurate prediction of soot volume fractions along the centreline up to x = 400 mm, within the soot formation region, are achieved when the differential diffusion effect is considered. Beyond this height, however, the calculated soot volume fraction in the oxidation zone evolves at a slower rate than observed in the experiment, leading to slightly higher predicted soot concentrations. This could be due to a lower soot oxidation rate produced in the CMC-based soot model than observed in the experiments, although no such under-prediction of oxidation rates is evident in the results for flame KH, nor indeed in flame YM examined later in this study. This discrepancy could be explained by comparing measured soot concentration distributions on the centreline between flame KH and flame CJ. Inspection of measured soot distributions on the centreline of flame KH, shown in Fig. 2, tends to confirm that the rate of soot formation is comparable with the rate of soot oxidation. The CMC-based soot model satisfactorily predicts the soot distribution in this flame in both of these zones. In contrast, the measured soot distribution on the centreline of flame CJ, presented in Fig. 3, indicates a rate of soot oxidation higher than that of soot formation, as reflected by a sharp fall-off of soot concentration after reaching its peak value. This is in accord with the experimental observation, reported by Coppalle and Joyeux (1994), which compared three ethylene flames of different Reynolds numbers and found that the flame considered in the present study has the highest oxidation rate among the three flames investigated.

Comparisons between predicted and measured radial profiles of soot volume fraction at two different axial locations for flame CJ are also presented in Fig. 3. An improvement in soot volume fraction predictions is again achieved when the CMC-based soot model accounts for the influence of differential diffusion. The radial position of the maximum soot volume fraction at x = 228 mm, as well as the overall shape of the soot profile at both axial positions, is seen to agree well with the data.

Flame YM represents the final flame investigated in this study. Restriction of space precludes presentation of graphs depicting flow and temperature fields for this flame. The results showed that although the calculated centreline mean mixture fraction is in very good agreement with the measurements, the predicted axial temperature is less conforming. In the lower parts of the flame, particularly in the range between 150 and 350 mm above the nozzle, the temperature is over-predicted by up to 200 K. However, outside this range the temperature is in good agreement with data. A similar discrepancy is also noted by Ma et al. (2005), and Mauss et al. (2006) when modelling this flame using a flamelet approach.

Figure 4 presents axial and radial profiles of predicted and measured soot volume fractions. Inspection of the axial profile again shows that improved soot predictions can be achieved by incorporating the differential diffusion effect of soot particles into the CMC model. The shape of the soot volume fraction distribution is identical to the measurements, although a lower prediction is obtained in the soot oxidation region. In comparison, Bai et al. (1998) slightly over-predicted soot concentrations in the oxidation region, with improved agreement with data obtained when the rate of particle inception was decreased by 20 percent. It should be noted that no adjustment was made in the present study either to the soot inception or oxidation rate. Without such an adjustment, the results demonstrate a similar level agreement with data to those of Ma et al. (2005) and Mauss et al. (2006).

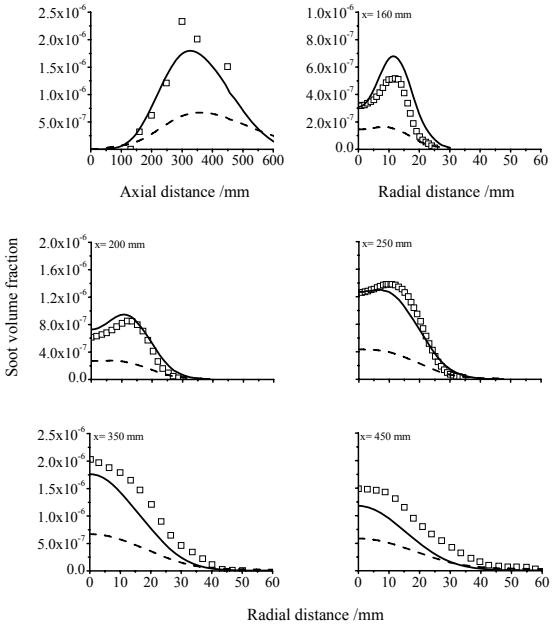

Fig. 4: Axial and radial soot volume fraction profiles for flame YM. Notation as in Fig. 2.

Radial soot predictions, given in the same figure, show that close to the nozzle, at x = 160 mm, the soot level is somewhat over-predicted, but the shape and peak location are in agreement with data. Soot predictions at the heights of x = 200 and 250 mm are in excellent agreement with the data. CMC predictions also demonstrate greater accord with the data when compared to results obtained at the same height of x = 250 mm in other studies (Ma et al., 2005; Mauss et al., 2006). Further downstream the predicted radial soot profiles still follow the pattern of the measurements, although soot volume fractions are slightly under-predicted at all radial locations. As with the previous flames considered, predictions that do not account for differential diffusion effects do not capture the experimental data

CONCLUSIONS

A first-order CMC-based soot model has been applied to the calculation of soot levels in three turbulent non-premixed ethylene flames, with one aim being to investigate the influence of differential diffusion of soot particles on predictions. The results demonstrate that predictions are in

better accord with data when such effects are accounted for, with predictions in the soot formation and oxidation zones of the flames in good agreement with observations, apart from in the strongly soot oxidising flame CJ which shows differences between predicted and measured soot values in the oxidation zone. Predictions that ignore differential diffusion significantly under-predict soot levels. Results therefore support the importance of accounting for the differential diffusion of soot particles in predicting sooting flames, as previously noted by Kronenburg et al. (2000).

In general, predictions of mean mixture fraction, temperature and soot volume fraction in the flames studied show good qualitative and quantitative agreement with data, and compare favorably with the results of earlier investigations of these flames that employed flamelet and transported PDF approaches. With respect to axial temperature predictions, an over-prediction occurred in the far-field region of flame KH, and within the lower part of flame YM, although an excellent representation of temperatures is obtained along the core of flame CJ, indicating that the radiation model employed is satisfactory. The use of Reynolds stress turbulence closures may be required in CMC calculations to improve the centerline temperature prediction in some flames.

REFERENCES

Bai, X.S., Balthasar, M., Mauss, F., and Fuchs, L., 1998, "Detailed Soot Modelling in Turbulent Jet Diffusion Flames", Proceedings of the Combustion Institute, Vol. 27, pp. 1623–1630.

Barlow, R.S., Smith, N.S.A., Chen, J.-Y., and Bilger, R.W., 1999, "Nitric Oxide Formation in Dilute Hydrogen Jet Flames: Isolation of the Effects of Radiation and Turbulence-Chemistry Submodels", Combustion and Flame, Vol. 117, pp. 4-31.

Brown, P.N., Byrne, G.D., and Hindmarsh, A.C., 1989, "VODE, a Variable-Coefficient ODE Solver", SIAM Journal on Scientific and Statistical Computing, Vol. 10, pp. 1038-1051.

Coppalle, A., and Joyeux, D., 1994, "Temperature and Soot Volume Fraction in Turbulent Diffusion Flames: Measurements of Mean and Fluctuating Values", Combustion and Flame, Vol. 96, pp. 275-285.

Fairweather, M., and Woolley, R.M., 2003, "First-Order Conditional Moment Closure Modelling of Turbulent, Nonpremixed Hydrogen Flames", Combustion and Flame, Vol. 133, pp. 393-405.

Fairweather, M., and Woolley, R.M., 2004, "First-Order Conditional Moment Closure Modelling of Turbulent, Nonpremixed Methane Flames", Combustion and Flame, Vol. 138, pp. 3-19.

Girimaji, S.S., 1991, "Assumed β-pdf Model for Turbulent Mixing: Validation and Extension to Multiple Scalar Mixing", Combustion Science and Technology, Vol. 78, pp. 177-196.

Kee, R.J., Rupley, F.M., and Miller, J.A., 1996, "CHEMKIN II: A FORTRAN Chemical Kinetics Package for the Analysis of Gas-Phase Chemical Kinetics", Report No. SAND89-8009B, Sandia National Laboratories.

Kent, J.H., and Honnery, D., 1987, "Soot and Mixture Fraction in Turbulent Diffusion Flames", Combustion Science and Technology, Vol. 54, pp. 383-397.

Kim, I.S., and Mastorakos, E., 2005, "Simulations of Turbulent Lifted Jet Flames with Two-Dimensional Conditional Moment Closure", Proceedings of the Combustion Institute, Vol. 30, pp. 905-912.

Klimenko, A.Yu., and Bilger, R.W., 1999, "Conditional Moment Closure for Turbulent Combustion", Progress in Energy and Combustion Science, Vol. 25, pp. 595-687.

Kronenburg, A., and Bilger, R.W., 2001a, "Modelling Differential Diffusion in Nonpremixed Reacting Turbulent Flow: Application to Turbulent Jet Flames", Combustion Science and Technology, Vol. 166, pp. 175-194.

Kronenburg, A., and Bilger, R.W., 2001b, "Modelling Differential Diffusion in Nonpremixed Reacting Turbulent Flow: Model Development", Combustion Science and Technology, Vol. 166, pp. 195-227.

Kronenburg, A., Bilger, R.W., and Kent, J.H., 2000, "Modeling Soot Formation in Turbulent Methane-Air Jet Diffusion Flames", Combustion and Flame, Vol. 121, pp. 24-40.

Leung, K. M., Lindstedt, R. P., and Jones, W. P., 1991, "A Simplified Reaction Mechanism for Soot Formation in Nonpremixed Flames", Combustion and Flame, Vol. 87, pp. 289-305.

Lindstedt, R.P., 1994, "Simplified Soot Nucleation and Surface Growth Steps for Nonpremixed Flames", In Soot Formation in Combustion, Bockhorn, H., ed., Springer-Verlag, Berlin, pp. 417-441.

Lindstedt, R.P., and Louloudi, S.A., 2005, "Joint-Scalar Transported PDF Modeling of Soot Formation and Oxidation", Proceedings of the Combustion Institute, Vol. 30, pp. 775-783.

Ma, G., Wen, J.Z., Lightstone, M.F., and Thompson, M.J., 2005, "Optimization of Soot Modelling in Turbulent Nonpremixed Ethylene/Air Jet Flames", Combustion Science and Technology, Vol. 177, pp. 1567-1602.

Mauss, F., Netzell, K., and Lehtiniemi, H., 2006, "Aspects of Modelling Soot Formation in Turbulent Diffusion Flames", Combustion Science and Technology, Vol. 178, pp. 1871-1855.

Pitsch, H., Riesmeier, E., and Peters, N., 2000, "Unsteady Flamelet Modeling of Soot Formation in Turbulent Diffusion Flames", Combustion Science and Technology, Vol. 158, pp. 389-406.

Qin, Z., Lissianski, V.V., Yang, H., Gardiner, W.C., Davis, S.G., and Wang, H., 2000, "Combustion Chemistry of Propane: A Case Study of Detailed Reaction Mechanism Optimization", Proceedings of the Combustion Institute, Vol. 28, pp. 1663-1669.

Spalding, D.B., 1977, "GENMIX: A General Computer Program for Two-dimensional Parabolic Phenomena", Pergammon Press, Oxford.

Wen, Z., Yun, S., Thomson, M.J., and Lightstone, M.F., 2003, "Modeling soot formation in turbulent kerosene/air jet diffusion flames", Combustion and Flame, Vol. 135, pp. 323–340.

Young, K.J., and Moss, J.B., 1995, "Modelling Sooting Turbulent Jet Flames using an Extended Flamelet Technique", Combustion Science Technology, Vol. 105, pp. 33-53.